Effect of zinc, magnesium, and copper substitutions on the initial permeability of nickel ferrite

SAREH SHAFIEE
Malek-Ashtar University of Technology
Ali Arab (aa.arab@yahoo.com)
Malek-Ashtar University of Technology
NASTARAN RIAHI-NOURI
Niroo Research Institute

Research Article

Keywords: Mg2+, Zn2+, and Cu2+ Substitution, Auto combustion, Initial permeability, High frequency, Particle size, Cations distribution

Posted Date: August 17th, 2020

DOI: https://doi.org/10.21203/rs.3.rs-57430/v1

Abstract

Zinc, magnesium, and copper substituted nickel spinel ferrite were synthesized in the form of $Ni_{1-x}(Zn_{06}Mg_{0\cdot2}Cu_{0.2})_x Fe_2O_4$ (where x = 0.0, 0.3, 0.5 and 0.7) via auto combustion method. The effect of the presence of these dopants on the average of crystallite, average particle size, the lattice constant, morphology, initial permeability, and magnetization of the synthesized ferrites was investigated. The structural properties, morphology, and magnetic properties were characterized via X-ray diffraction (XRD), field emission scanning electron microscopy (FE-SEM), energy dispersive spectroscopy (EDS), LCR meter and alternative gradient force magnetometer (AGFM). XRD study shows the formation of a single-phase cubic spinel structure. Also, the average crystallite size was found to increase from 6 nm to 11 nm with increasing the Zn^{2+}, Mg^{2+}, and Cu^{2+} doping ratio from 0.0 to 0.7. Moreover, FE-SEM results were indicated the presence of nanosized spherical shape of prepared particles with agglomeration. The lattice constant and the particle size were found to increase with the increase in Zinc, magnesium, and copper. The values of initial permeability and magnetization were increased to a maximum value of 76 H/M and 71.37 emu/g for x = 0.7 sample. Furthermore, coercivity was found to decrease with increasing Zinc, magnesium, and copper concentration, which is useful for power applications. The variations of initial permeability and magnetization as a function of average particle size were discussed and were compared with previous works. The results were indicated the increase in initial permeability and magnetization with the enhancement of average particle size. The constancy in permeability throughout the frequency range studied from 10 kHz to1 MHz was indicated the compositional stability and quality of the samples. The results were indicated that the ferrites with high initial permeability can be an excellent choice as magnetic cores.

1. Introduction

ZnMgCu-substituted nickel ferrites have been indicated excellent magnetic properties in the high-frequency from several kHz to MHz [1]. They are applied in power supply transformers, choke coils, power transformers, and noise filters [1]. The lattice of oxygen ions in spinel ferrite determines the structure and morphology of ferrites. The radii of oxygen ions are larger than the metal ions [2, 3]. The tetrahedral (A) and octahedral (B) sites are surrounded by 4 and 6 oxygen ions, respectively. Electrical and magnetic properties of ferrites are dependent on cationic distribution, composition, and nature of impurity ions in the material [4]; the structural properties of ferrites are dependent on compositions and synthesis methods [5]. The growth of grains is influenced by grains' boundary mobility. Recrystallization and the growth of grains cause the movement of grain boundaries and the increase in initial permeability [6]. To improve the electronic and magnetic properties of ferrites numerous divalent cations, such as chromium, copper, manganese, and zinc, substitute on ferrites [4]. The auto combustion method in comparison with others is more acceptable for synthesizing ferrites due to the high sintering, homogenous particle size distribution, and lower time consumed [7]. This method is rather simple, safe, and economical [8]. Zn^{2+} ions have a strong preference to occupy the A sites [9], whereas the Ni^{2+} ions have a strong preference to occupy the B sites. Therefore, with increasing Ni^{2+} substitution on Zn ferrite, Fe^{3+} ions in B sites, due to the occupancy of B sites by Ni^{2+} ions, migrate to A sites [10]. Previous studies have reported the synthesize of CuMgZnNi-ferrites. Thorat et al. has investigated the initial permeability and magnetic properties of $Mg_{0.25-x}Ni_xCu_{0.25}Zn_{0.5}Fe_2O_4$; reported that the initial permeability reaches the maximum value μ = 2620 at x = 0.05 [11]. Gangaswamy et al. investigated the magnetic behavior of $Ni_{0.65-x}Mg_xZn_{0.35}Fe_2O_4$; reported that the Mg substitution enhances the saturation magnetization [6]. Roy et al. has studied the electromagnetic properties of

$Ni_{0.25-x}Mg_xCu_{0.2}Zn_{0.55}Fe_2O_4$ ferrite prepared by the auto combustion method; reported that the very high permeability of $Ni_{0.07}Mg_{0.18}Cu_{0.2}Zn_{0.55}Fe_2O_4$ due to better densification, lower magnetostriction constant and inner stresses [12].

In this work, $Ni_{1-x}(Zn_{06}Mg_{0\cdot2}Cu_{0.2})_x Fe_2O_4$ have prepared by the auto combustion method. The aim of this work is: (1) to find the regularities of the effect of zinc, magnesium, and copper substitutions on the initial permeability of $NiFe_2O_4$ spinel ferrite; (2) investigate the morphological, structural and magnetic features of ferrite samples; (3) discuss the application of ferrite samples in high-frequency and the variations initial permeability as a function of particle size. The samples prepared in this work displayed a considerable performance in soft magnetic characteristics and high-frequency permeability.

2. Experimental

2.1. Samples preparation

A series of ZnMgCu-substituted nickel ferrites with the formula of $Ni_{1-x}(Zn_{06}Mg_{0\cdot2}Cu_{0.2})_x Fe_2O_4$ (x = 0.0, 0.3, 0.5 and 0.7) were made by the auto combustion method. The preparation of nanopowders had been revealed in previous work [12]. A stoichiometric ratio of Merck materials $Zn(NO_3)_2.6H_2O$, $Cu(NO_3)_2.3H_2O$, $Mg(NO_3)_2.6H_2O$, $Ni(NO_3)_2.6H_2O$, and $Fe(NO_3)_2.9H_2O$ with purity ≥ 98% were dissolved in water deionized using a magnetic stirrer. Then, the $NH_5C_2O_2$ solution was added to the mixtures slowly. The mixture was heated at a temperature of 80°C – 200°C for two hours with continuous stirring. The obtained gel was dried at 250°C for two hours. Then the prepared powders were calcined at 600°C for four hours.

The powders were granulated using polyvinyl alcohol (PVA) as a binder and were pressed at a pressure of 3 ton/cm^2 into toroidal shape (about 4 mm diameter and 3 mm thickness). The toroid samples were sintered at 900°C for 8 h in air and were wound by copper wire at room temperature.

2.2. Characterization

The powders were characterized by XRD (X' Pert Pro MPD model), where the wavelength of Cu K_α radiation was 1.54 Å. Their morphology was carried out by FESEM (Hitachi S- 4160 model). The compositions of the ferrites were measured through energy-dispersive x-ray spectroscopy (EDS). The initial permeability of toroid ferrites was measured by L.C.R meter (Hioki IM3536 model) in the frequency range from 10 kHz to 10 MHz. while the magnetic properties were characterized by AGFM in a maximum field of 9 kOe.

3. Results And Discussion

3.1. Analysis of structure and composition

Fig. 1 shows the X-ray diffraction (XRD) patterns of $Ni_{1-x}(Zn_{0.6}Mg_{0.2}Cu_{0.2})_x Fe_2O_4$ (x= 0.0, 0.3, 0.5 and 0.7) samples. It can be seen that the prominent hkl planes (220), (311), (222), (400), (422), (511), and (440) were identified. The patterns were confirmed the formation cubic spinel structure of samples due to the well matching with the standard XRD patterns (JCPDS PDF cars No. 00-008-0234). Similar results have been revealed in previous work [13, 14]. The average crystallite size (D) was calculated by using the Scherer-Debye equation [15]:

$$D = \frac{0.9\lambda}{\beta \cos\theta} \quad (1)$$

D is the average crystallite size, θ is the Bragg's diffraction angle, λ is incident beam wavelength, $\beta = (\beta^2_{exp} - \beta^2_{std})^{1/2}$, β_{exp} and β_{std} are FWHM peaks and the standard, respectively.

The lattice constant (a) was calculated by using Bragg's equation [16]:

$$a = d\,(h^2 + k^2 + l^2)^{\frac{1}{2}} \quad (2)$$

Where "a" is the lattice constant, d is inter planer spacing, (hkl) are Miller indices of respective peaks.

From Table 1 which shows XRD parameters of ferrites can be seen that the average crystallite size raised from 6 nm to 11 nm with increasing the doping ratio of magnesium, copper, and zinc. The increase in the average crystallite size may be due to the liquid phase in the calcination process. With the addition of Zn^{2+}, Mg^{2+}, and Cu^{2+} ions, the contact area of solid reaction increases, and the growth of the crystallite size accelerates [18]. Also, the lattice constant found to be increased little from 8.331 Å to 8.372 Å with increasing the x content (0.0 to 0.7). The lattice constant is dependent on the difference between the substitution ions and host ions radii and the cationic distribution among the interstitial tetrahedral (A) and octahedral (B) sites [18]. The increase in lattice constant is due to larger ionic radii of Cu^{2+} (0.73 Å), Mg^{2+} (0.72 Å) and Zn^{2+} (0.82 Å) than nickel (0.69 Å) [19]. This agrees with other works observed byWhere "a" is the lattice constant, d is inter planer spacing, (hkl) are Miller indices of respective peaks.

Roy et al. [12] and Thorat et al. [11]. The variations in lattice constant and crystallite size as x contents are shown in Fig. 2.

Fig. 3 indicates the FE-SEM micrographs for all the samples. The substitution of Cu, Mg, and Zn ions into nickel ferrites has influenced on their size and structure. The average particle size increases with the addition of Cu, Mg, and Zn ions from 21 nm to 26 nm, as listed in Table 1. The spherical nature of the particles and the agglomeration of grains is shown in the FE-SEM images. The variation in particle size as x concentration are shown in Fig. 4. The increase in lattice volume has an important role in grain boundary diffusion [20]. With increasing lattice volume, the diffusion path, and the rate of the cation interdiffusion increase. Furthermore, the growth of grain is related to the grain's boundary mobility [21]. Recrystallization and grains growth lead to the movement of grains boundaries and the variations in permeability, density, and resistivity [21]. So, the grain boundary diffusion was increased by increasing Cu^{2+}, $Mg^{2+,}$ and Zn^{2+} substitutions.

Using EDS, the distribution of elements in selected samples with x= 0.3, 0.5 were analyzed. The atomic percentage of elements are given in Fig. 5. The spectra confirmed that the final compositions of ferrites were the same as those of compositions without any extra impurity elements.

3.2. Analysis of magnetic performance

Fig. 6 shows the initial permeability (μ) as a function of frequency for $Ni_{1-x}(Zn_{06}Mg_{0\cdot2}Cu_{0.2})_x Fe_2O_4$ (x=0.0, 0.3, 0.5 and 0.7) ferrites under the frequency range of 10 kHz-10 MHz. As depicted clearly, μincreases with the increasing zinc, magnesium, and copper and reaches the maximum value μ= 76 at x= 0.7. The increase in initial permeability has been attributed to grain size. The variations of the initial Permeability as a function of x concentration and particle size in the frequency range of 10 kHz- 10 MHz are shown in Fig. 7 and Fig. 8. The observed variation in initial permeability can be due to the basis of changes that took place in grain size as evident from FE-SEM micrographs. The variations in initial permeability are parallel to the changes observed in the particle size. The initial permeability correlates by two different magnetizing mechanisms of ferrites; the movement of domain wall and the spin rotation [22]. The spin rotation is smaller than domain walls at the low-frequency region, the domain wall movement is reversible because of the presence of a weak magnetic field [21, 23].

As can see in Fig. 8, the increase in particle size causes an increase in domain wall contribution, and the increasing initial permeability [24]. It is a well-known fact that the increase in grain size reduces the number of grain boundaries in a sample and causes an increase in the initial permeability [25]. The higher μobtained for the composition x = 0.7 at the frequency of 10 kHz is contributed by the domain wall oscillations in the bigger grains of this composition. Furthermore, the μremained steady over a wide range of frequency 10 kHz -1 MHz, and then decreases rapidly greater than 1 MHz applied frequency, as indicated in Fig. 6. The stability of μ from 10 kHz to 1 MHz is due to the domain wall motion. The frequency of 1 MHz is named the zone of utility [26], which is equal to the external magnetic field frequency and a desirable characteristic for various applications of ferrites in high-frequency, such as broadband pulse transformers and wideband read-write heads for video recording [26]. After the resonance frequency (1 MHz) the μ decreases due to the absorption of magnetic energy by spin moments [24]. The required energy for the displacement of the domain wall is lower than that required for domain rotation. The constancy in permeability throughout the frequency range studied from 10 kHz to1 MHz indicates the compositional stability and quality of the samples. The present investigation of Cu^{2+}, $Mg^{2+,}$ and Zn^{2+} substituted Ni ferrites reveal that the ferrites with the high initial permeability are an excellent choice as magnetic cores.

The characteristics of μhave been reported by Roy et al. [12] for Ni-Zn-Mg-Cu ferrites prepared by the auto combustion method and Thorat et al. [11] for Ni-Zn-Mg-Cu ferrites prepared by citrate assisted sol-gel method, which agrees with our reported values. The results are listed in Table 2.

The initial permeability is influenced by compositions, impurity contents, preparation methods, grain size, saturation magnetization, magnetostriction [17, 22]. The μvalues reported by Roy et al. [12] and Thorat et al. [11] are higher than those obtained for the $Ni_{1-x}(Zn_{0.6}Mg_{0.2}Cu_{0.2})_x Fe_2O_4$ in the present investigation. It may be due to the different preparation methods and the higher calcination and sintering temperature of samples than those ferrite samples in the present investigation. The density and grain size of the ferrites increase with increasing sintering temperature, and they would affect magnetic properties directly [27]. Higher crystallite and particle sizes, and higher temperature used for calcination and sintering samples cause to increase in μ. The magnetization mechanism of soft magnetic materials is domain wall motion, which generates high initial permeability (μ). Although pores and grain boundary would obstruct the movement of the domain wall, the fewer amounts of pores and grain boundary could be obtained at higher sintering temperature and lead to easy movement of domain wall

and high initial permeability [27]. Furthermore, the values of μ reported by Roy et al. [12] indicated that the increase in permeability is attributed to the increase in particle size.

Fig. 9 illustrates the magnetization (M) as a function of field (H) curves for the $Ni_{1-x}(Zn_{0.6}Mg_{0.2}Cu_{0.2})_xFe_2O_4$ (x=0.0, 0.3, 0.5 and 0.7) ferrite at room temperature and maximum magnetic field of 9 kOe. The magnetization is not saturated until 9 kOe in all hysteresis curves. From the plotted M-H curves, the maximum magnetization (M), and coercivity (H_c) were measured as reported in Table 1. With increasing Cu^{2+}, Mg^{2+}, and Zn^{2+} ions in the nickel ferrite the magnetization increases. The increase in magnetization can be due to the variations of exchange interactions between A and B sites, an increase in the crystalline nature, and a narrow particle size distribution [26]. The magnetization is calculated about 57.94 emu/g, 68.41 emu/g, and 71.37 emu/g for samples with x= 0.3, 0.5, and 0.7 respectively, which are higher than that of the unsubstituted nickel ferrite sample (32.5 emu/g). Moreover, the M value of ferrite with x=0.7 is higher than that of the substituted nickel ferrite samples. The magnetic properties are influenced by the composition and different cation distribution as described by the Neel model [24]. According to Neel's theory, the net magnetic moment can be defined as following [24]:

$$M=|M_B-M_A| \quad (3)$$

Where M_A and M_B are the magnetic moments of A and B sublattices [24].

The replacement of cations substituted in the spinel ferrites leads to weak or strong interaction among magnetic ions [13]. It is reported in previous research that the Zn^{2+} and Mg^{2+} ions have a strong preference for occupancy the A sites; the Ni^{2+} and Cu^{2+} ions have a strong preference towards B sites, while the Fe^{3+} ions distribute over both A and B sites [28, 29]. The magnetic moment of Zn^{2+}, Cu^{2+}, Ni^{2+}, Fe^{+3} and Mg^{2+} ions is 0, 1.3, 2.3, 5 and 0 μ_B, respectively [15, 19]. With the increasing of Cu^{2+}, Mg^{2+}, and Zn^{2+} ions on nickel ferrite, the copper ions occupy B sites, due to their high preference towards B sites, and a smaller concentration of copper may appear at A sites. The diamagnetic Zn^{2+} and Mg^{2+} ions occupy the A sites, where cause the movement of Fe^{3+} ions from A sites to B sites. Therefore the increase in magnetization is due to the higher magnetic moment of B than A sublattices [30]. The variations of magnetization and coercivity of ferrite samples as a function of x are shown in Fig. 10.

The magnetic characteristics are dependent on the particle size, anisotropy, density, cationic stoichiometry, random canting of particle spins, and surface effects [29, 31]. The increase of M can be explained with the particle size trend. As reported in the structural analysis of this series published elsewhere, the particle size has increased with an increase in the amount of doped copper, zinc, and magnesium. The variation of magnetization and coercivity dependence of average particle size is shown in Fig. 11. As can be seen the magnetization increases by the enhancement of particle size. As the particle size increases, the number of magnetic domains increases, and the movement of the domain wall facilitates, which leads to the enhancement of magnetization [32]. This behavior can also be justified according to the core-shell model [33]. In this model, each particle consists of a magnetically ordered core and a spin glass surface with a constant thickness without net magnetization [33]. The disordering of the surface layer spins may be due to the broken super-exchange bonds and unlike local symmetry for those atoms near the surface layer [33]. In smaller particles, the surface to volume ratio of particles is higher, which leads to a decrease in magnetization [33]. With an increase in the average particle size, due to the diminution in the surface to volume ratio, the magnetization increases.

Coercivity (H_c) gives the value of the applied field, at which the induced magnetization is zero. The values of H_c for ferrite samples are listed in Table 1. As can be seen from Fig. 10 the coercivity decreases with Cu^{2+}, $Mg^{2+,}$ and Zn^{2+} substitution. The H_c is dependent on the particle size, grain boundaries, anisotropy, and precipitates [34]. The increase in particle size of ferrites decreases the surface area to volume ratio and surface anisotropy of the crystal. The coercivity property of the samples originates from a multi-domain structure. In the multi-domain region, the increase in particle size decreases the coercivity [35]. Referring to the variations of M and μ as a function of average particle size, it is understood that the dependence of magnetization to the initial permeability is direct. Therefore, the increase in particle size leads to an increase in domain wall contribution and an increase in initial permeability [24].

4. Conclusion

Cu^{2+}, Mg^{2+}, and Zn^{2+} doing nickel ferrites have been successfully prepared by the auto combustion method. XRD results confirmed the formation of a cubic spinel structure. With increasing zinc, magnesium, and copper the crystallite size and lattice constant increased. FE-SEM analysis reported the spherical shape of ferrite nanoparticles along with the presence of high agglomeration due to magnetic interactions between ferrites particles. Also, the average particle size increased by addition zinc, magnesium, and copper on nickel ferrite. In the ferrite sample of $Ni_{0.3}Zn_{0.42}\ Mg_{0.14}\ Cu_{0.14}\ Fe_2\ O_4$ the average crystallite size, the lattice constant and particle size be larger than maybe understood due to larger ionic radii of Cu^{2+}, Mg^{2+}, and Zn^{2+} as compared to Ni^{2+}.

The initial permeability increased by increasing x content and average particle size at a frequency range of 10 kHz-10 MHz due to the grain growth. The constancy in initial permeability throughout the frequency range studied from 10 kHz to1 MHz, due to the contribution of domain wall motion, indicated the compositional stability and quality of the samples. The reduction of initial permeability from 1 MHz to 10 MHz, illustrated the external magnetic field frequency. The investigation of Cu^{2+}, $Mg^{2+,}$ and Zn^{2+} substituted Ni ferrites revealed that the ferrites with the high initial permeability are an excellent choice as magnetic cores. The μ values of present work compared with the results of previous work. The μ in other works were found to be higher than those obtained for the $Ni_{1-x}\ (Zn_{0.6}\ Mg_{0.2}Cu_{0.2})_{\ x}\ Fe_2O_4$ ferrites in the present investigation. It can be due to the different preparation methods and the higher calcination and sintering temperature of samples than those ferrite samples in the present investigation. The density and grain size of the ferrites increase with increasing sintering temperature, and they would affect magnetic properties directly. Furthermore, hysteresis loops showed an increase in magnetization, due to the site's occupation of Zn, Mg, and Cu ions, with the enhancement of Cu^{2+}, $Mg^{2+,}$ and Zn^{2+} ions. While the coercivity decreased due to a multi-domain structure of ferrites. The M and μ influenced by the average particle size, due to the variation of the surface to volume ratio of particles. From the results of all characterization techniques in this paper, it is concluded that the sample of $Ni_{0.3}Zn_{0.42}\ Mg_{0.14}\ Cu_{0.14}\ Fe_2\ O_4$, due to the higher M and μ, can be used as a magnetic core. Also, it can be applied in various technologies useful in many fields like medical, information and communication, etc. The obtained results were compared with previous works.

Declarations

Acknowledgments

This study was completed at Malek Ashtar University of technology and was supported by Niroo Research Institute. The authors are grateful to the institute for their support.

References

1. Satoshi G, Toshiaki O, Yutaka F, Jirou T, High-Performance MnZn Ferrites for Transformer Core Used in forwarding Mode Switching Power Supply, J. JFE. Tech. Repo. 16 (2011).CrossRef
2. Rahman MdT, Vargas M, Ramana CV (2014) Structural characteristics, electrical conduction, and dielectric properties of gadolinium substituted cobalt ferrite. J Alloy Compd 617:547–562. CrossRef
3. Meng YY, Liu ZW, Dai HC, Yu HY, Zeng DC, Shukla S, Ramanujan RV (2010) Powd. Tech, Structure, and magnetic properties of Mn(Zn)$Fe_{2-x}RE_xO_4$ ferrite nano-powders synthesized by co-precipitation and refluxing method. J pow Tech 229:270–275.CrossRef
4. Gholizadeh A, Jafari E (2017) Effects of sintering atmosphere and temperature on structural and magnetic properties of Ni-Cu-Zn ferrite nano-particles: Magnetic enhancement by a reducing atmosphere. J Magn Magn Mater 422:328–336.CrossRef
5. Saafan SA, Meaz TM, El- Ghazzawy EH, El-Nimr MK, Ayad MM, Bakr M (2010) A.C. and D.C. conductivity of NiZn ferrite nanoparticles in wet and dry conditions. J Magn Magn Mater 322:2369–2374. CrossRef
6. Gangaswamy DRS, Chaitanya Varma M, Bharadwaj S, Sambasiva Rao K, Rao KH (2015) Comparison study of structural and magnetic properties of magnesium-substituted nickel-zinc ferrites synthesized by solid-state and sol-gel routes. J Supercond Nov Magn 28:3599. CrossRef
7. Ramesh S, Dhanalakshmi B, Sekhar BC, Rao PSVS, Rao BP (2016) Effect of Mn/Co substitutions on the resistivity and dielectric properties of nickel-zinc ferrites. J Ceram Int 42:9591–9598. CrossRef
8. Li X, Wang G (2009) Low-temperature synthesis and growth of superparamagnetic $Zn_{0.5}Ni_{0.5}Fe_2O_4$ nanosized particles. J Magn Magn Mater 321:1276–1279.CrossRef
9. Parvatheeswara Rao B, Dhanalakshmi B, Ramesh S, Subba Rao PSV (2018) Cation distribution of Ni-Zn-Mn ferrite nanoparticles. J Magn Magn Mater 456:444–450. CrossRef
10. Anwar H, Maqsood A, Comparison of structural and electrical properties of Co^{2+}doped Mn-Zn soft nano ferrites prepared via coprecipitation and hydrothermal methods. J. Mater. Res. Bull. 49 (2014) 426–433.CrossRef
11. Thorat LM, Patil JY, Nadargi DY, Ghodake UR, Kambale RC, S. S. Suryavanshi, Ni^{2+}-substituted Mg–Cu–Zn ferrites: a colloidal approach of tuning structural and electromagnetic properties, J. Sol. Sci. Tech, 2018. CrossRef
12. Roy PK, Bera J (2006) Effect of Mg substitution on electromagnetic properties of (Ni0.25Cu0.20Zn0.55)Fe2O4 ferrite prepared by auto combustion method. J Magn Magn Mater 298:38–42. CrossRef
13. Ati AA, Othaman Z, Samavati A (2013) Influence of cobalt on structural and magnetic properties of nickel ferrite nanoparticles. J Mol Struct 1052:177–182. CrossRef
14. Kumar GR, Kumar KV, Venudhar YC (2012) Synthesis, structural and magnetic properties of copper substituted nickel ferrites by sol-gel method. J Mattr Sci Appl 3:87–91. CrossRef
15. Tancharoen Th, Ruangphanit A, Pecharapa W (2013) Structural and magnetic properties of nanocrystalline zinc-doped metal ferrites (metal = Ni; Mn; Cu) prepared by sol-gel combustion method. J Ceram Int 39:S239-

S 243.CrossRef

16. Cullity BD, Grahm CD, Introduction to magnetic materials,2nd eds. (Hoboken: Wiley), 360 (2009). CrossRef
17. Bahiraei H, Ong CK (2016) Microstructural and electromagnetic study of low temperature fired MgCuZn ferrite with Bi_2O_3 addition. J Ceram Int 43:6. CrossRef
18. Jacobo SEP, Bercoff G (2016) Structural and electromagnetic properties of yttrium substituted Ni-Zn ferrites. J Ceram Int 42:7664–7668. CrossRef
19. Yoon DH (2016) K.Raju, Controlling the magnetic properties of nickel ferrites by doping with different divalent transition metal (Co, Cu, and Zn) cations. J Super Nove Magn 29:439–445. CrossRef
20. Shokrollahi H, Magnetic properties and densification of Manganese–Zinc soft ferrites (Mn1-xZnxFe2O4) doped with low melting point oxides, J. Mag. Mag. Mater. 320 (2008) 463. CrossRef
21. Lakshman A, Subba Rao PSV, Parvatheeswara Rao B, Rao KH (2005) Electrical properties of In^{3+} and Cr^{3+} substituted magnesium–manganese ferrites. J Appl Phys 38:673–678. CrossRef
22. Kesavamoorthi R, Ramachandra C, Raja, Structural and magnetic properties of cobalt and copper ions mixed nickel ferrite nanoparticles. J. Super. Nove. Magn, 2017. CrossRef
23. Ganga Swamy DRS, Chaitanya Varma M, Bharadwaj S (2015) Effect of magnesium on relaxation frequency of Ni–Zn nano ferrites. J Modern PhysB 29:1550218. CrossRef
24. Gangaswamy DRS, Choudary GSVRK, Chaitanya Varma M, Bharadwaj S, Rao KH, Enhanced Magnetic Permeability in $Ni_{0.55-y}Co_yZn_{0.35}Mg_{0.10}Fe_2O_4$ Synthesized by Sol-Gel Method, J. Super.condu. Novel. Mag, 2018. CrossRef
25. Ghodake JS, Shinde TJ, Patil RP, Patil SB (2015) S.S.Suryavanshie, Initial permeability of Zn–Ni-Co ferrite. J Magn Magn Mater 378:436. CrossRef
26. Verma A, Chatterjee R (2006) Effect of zinc concentration on the structural, electrical, and magnetic properties of mixed Mn–Zn and Ni–Zn ferrites synthesized by the citrate precursor technique. j Magn Magn Mater 306:313–320. CrossRef
27. Wei-Chih Hsu SC, Chen PC, Kuo CT, Lie WS, Tsai (2004) Preparation of NiCuZn ferrite nanoparticles from the chemical. J Mater Sci EngB 111:142–149. CrossRef
28. Balavijayalakshmi J, Suriyanarayanan N, Jayaprakash R (2015) Role of copper on structural, magnetic, and electric properties of nickel ferrite nanoparticles. J Magn Magn Mater 385:302–307. CrossRef
29. Shams Alam R, Moradi M, Rostami M, Nikmanesh H, Moayedi R, Bai Y, Structural, magnetic, and microwave absorption properties of doped Ba-hexaferrite nanoparticles synthesized by the co-precipitation method. J. Magn. Magn. Mater. 1 (2015) 381. CrossRef
30. Kargar Z, Asgarian SM, Mozaffari M, Positron annihilation, and magnetic properties of copper substituted nickel ferrite nanoparticles, j. Nuclear Instr. Methods in Phys. Res. B. 375 (2016) 71– 78. CrossRef
31. Sharifi I, Shokrollahi H (2013) Structural, Magnetic, and Mössbauer evaluation of Mn substituted Co–Zn ferrite nanoparticles synthesized by co-precipitation. Magn Magn Mater 334:36–40.CrossRef
32. Liu Z, Peng Z, Lv C, Fu X (2017) Doping effect of Sm^{3+} on magnetic and dielectric properties of Ni-Zn ferrites. J Ceram Int 43:1449–1454. CrossRef
33. Amighian M, mozaffari A, Arab A, Yousefi MH (2010) The effect of La-substitution on magnetic properties of nanosized $Sr_{1-x}La_x Ti_{0.05} Zn_{0.2}(Fe^{3+})_{11.75-\delta} (Fe^{2+})_{\delta} O_{19}$ powders. J Magn Magn Mater 322:748–752. CrossRef

34. Hasani S, Shamanian M, Shafyei A, Behjati P, Nezakat M, Fathi-Moghaddam M, Szpunar JA, Influence of annealing treatment on micro/macro-texture and texture dependent magnetic properties in cold rolled FeCo-7.15V alloy, J. Magn. Magn. Mater. 378 (2015).CrossRef
35. Hajalilou A, Hashim M, Ebrahimi-Kahrizsangi R, Mohamed H, Kamari (2015) Influence of evolving microstructure on electrical and magnetic characteristics in mechanically synthesized polycrystalline Ni-ferrite nanoparticles. J Alloys Compd 633:306–316. CrossRef

Tables

Table 1

The contents of D, a, d, μ, M, and H_c of $Ni_{1-x}(Zn_{0.6}\ Mg_{0.2}Cu_{0.2})_xFe_2O_4$ for different x values.

X	Samples	the average crystallite size (D) nm	Lattice constant (*a*) Å	Average particle size (d) nm	Initial permeability (μ) H/M 100 kHz-1 MHZ	Maximum magnetization (M) emu/g	Coercivity field (H_c) Oe
0.0	$NiFe_2O_4$	6	8.331	21	32	32.50	198.41
0.3	$Ni_{0.7}(Zn_{0.6}\ Mg_{0.2}Cu_{0.2})_{0.3}Fe_2O_4$	8	8.357	23	58	57.94	131.95
0.5	$Ni_{0.5}(Zn_{0.6}\ Mg_{0.2}Cu_{0.2})_{0.5}Fe_2O_4$	10	8.369	25	71	68.41	96.25
0.7	$Ni_{0.3}(Zn_{0.6}\ Mg_{0.2}Cu_{0.2})_{0.7}Fe_2O_4$	11	8.372	26	76	71.37	92.12

Table 2

The contents of D, a, d, μ reported by Roy et al. [12] and Thorat et al. [11] for different ferrite samples.

X	Samples	the average crystallite size (D) nm	Lattice constant (*a*) Å	Average particle size (d) nm	Initial permeability (μ) H/M 100 kHz-1 MHZ	Method of synthesis
0.0	$Ni_{0.18}Zn_{0.55}Mg_{0.7}Cu_{0.2}Fe_2o_4$	124	8.3990	-	680	
0.3	$Ni_{0.12}Zn_{0.55}Mg_{0.13}Cu_{0.2}Fe_2o_4$	121.9	8.3991	-	940	Auto combustion
0.5	$Ni_{0.7}Zn_{0.55}Mg_{0.18}Cu_{0.2}Fe_2o_4$	127.6	8.4097	-	2420	
0.7	$Ni_{0.5}Zn_{0.5}Mg_{0.2}Cu_{0.25}Fe_2O_4$	48	8.392	237	2620	
	$Ni_{0.1}Zn_{0.5}Mg_{0.15}Cu_{0.25}Fe_2O_4$	51	8.400	237	1930	citrate assisted sol-gel
	$Ni_{0.15}Zn_{0.5}Mg_{0.1}Cu_{0.25}Fe_2O_4$	47	8.405	338	1569	
	$Ni_{0.2}Zn_{0.5}Mg_{0.5}Cu_{0.25}Fe_2O_4$	49	8.407	180	522	

Figures

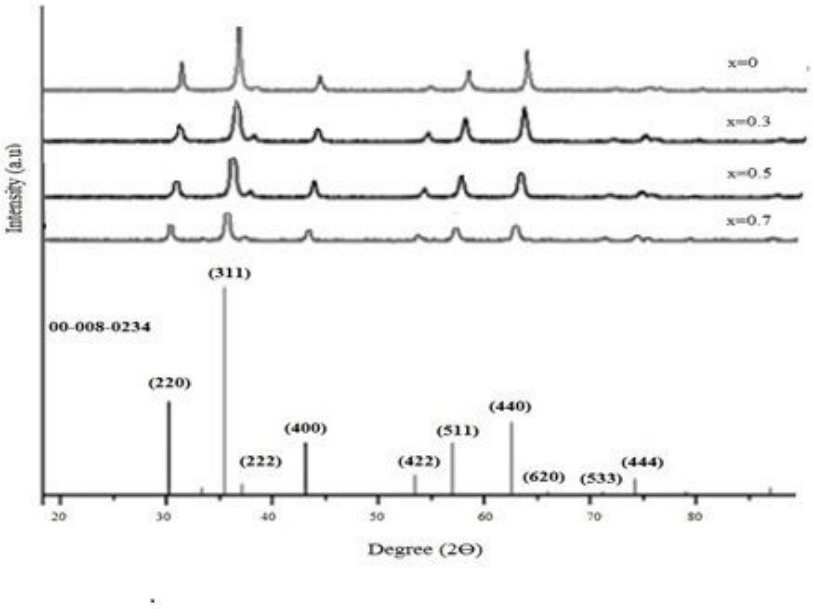

Figure 1

Indexed XRD patterns of Ni1-x (Zn0.6 Mg0.2Cu0.2) x Fe2O4with x equal to: 0.0, 0.3, 0.5 and 0.7.

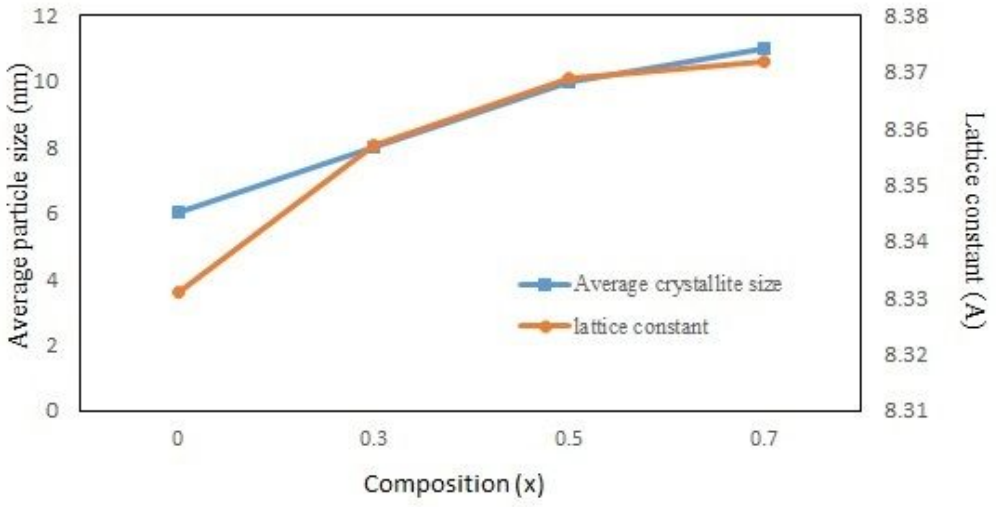

Figure 2

The variations of the lattice parameter and average crystallite size concerning x values for Ni1-x (Zn0.6 Mg0.2Cu0.2) x Fe2O4. Morphology of Ni1-x (Zn0.6 Mg0.2Cu0.2) x Fe2O4with x equal to: 0.0, 0.3, 0.5 and 0.7.

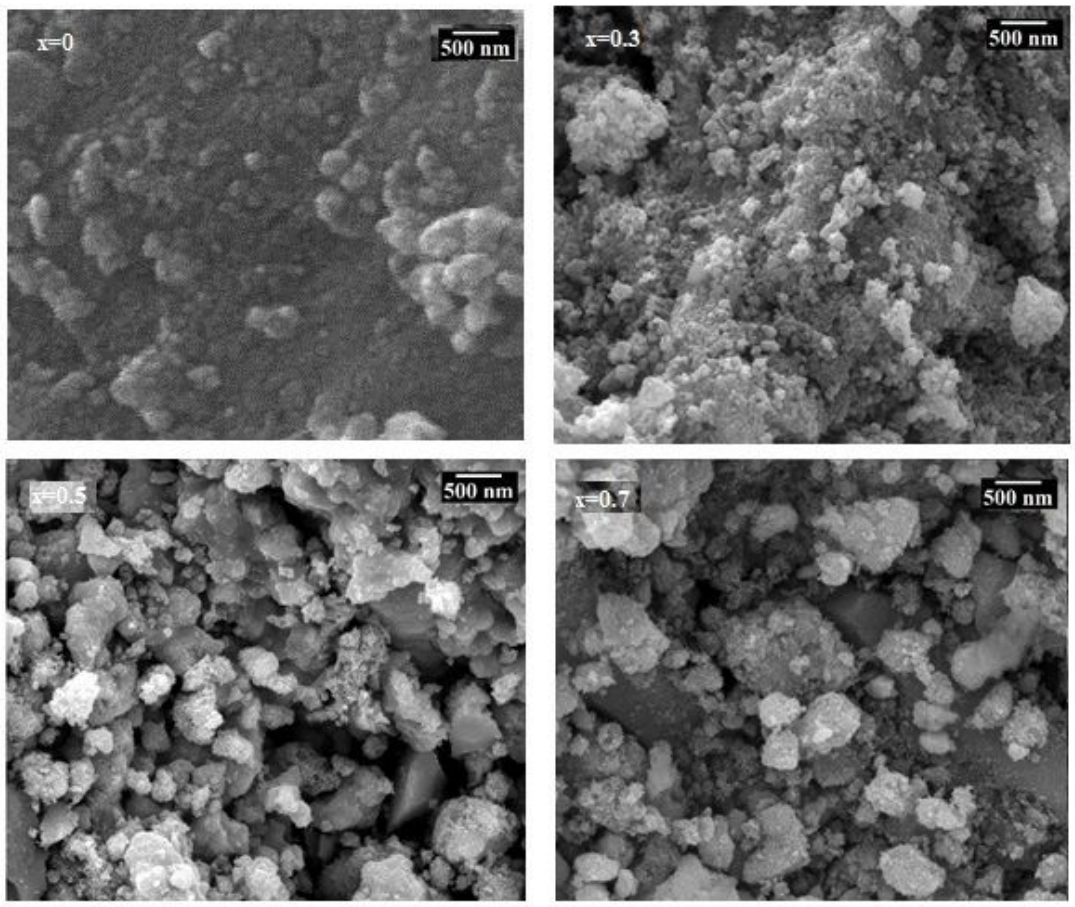

Figure 3

Morphology of Ni1-x (Zn0.6 Mg0.2Cu0.2) x Fe2O4with x equal to: 0.0, 0.3, 0.5 and 0.7.

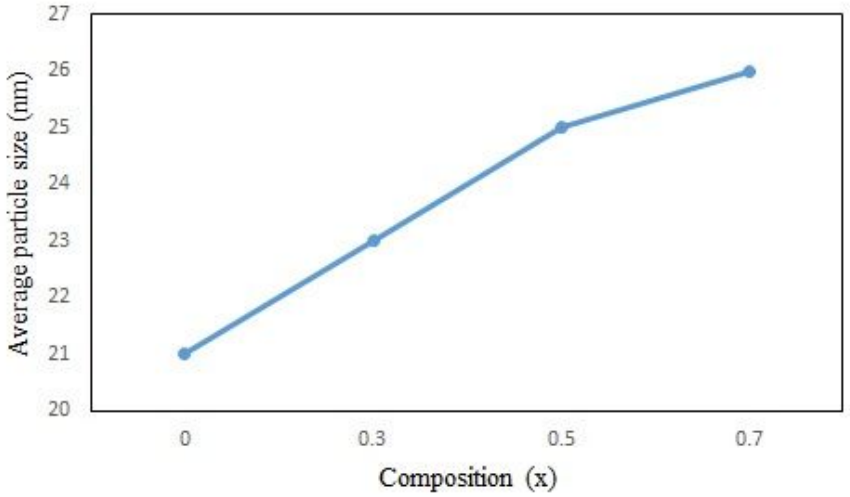

Figure 4

The variations of the average particle size concerning x values for Ni1-x (Zn0.6 Mg0.2Cu0.2) x Fe2O4.

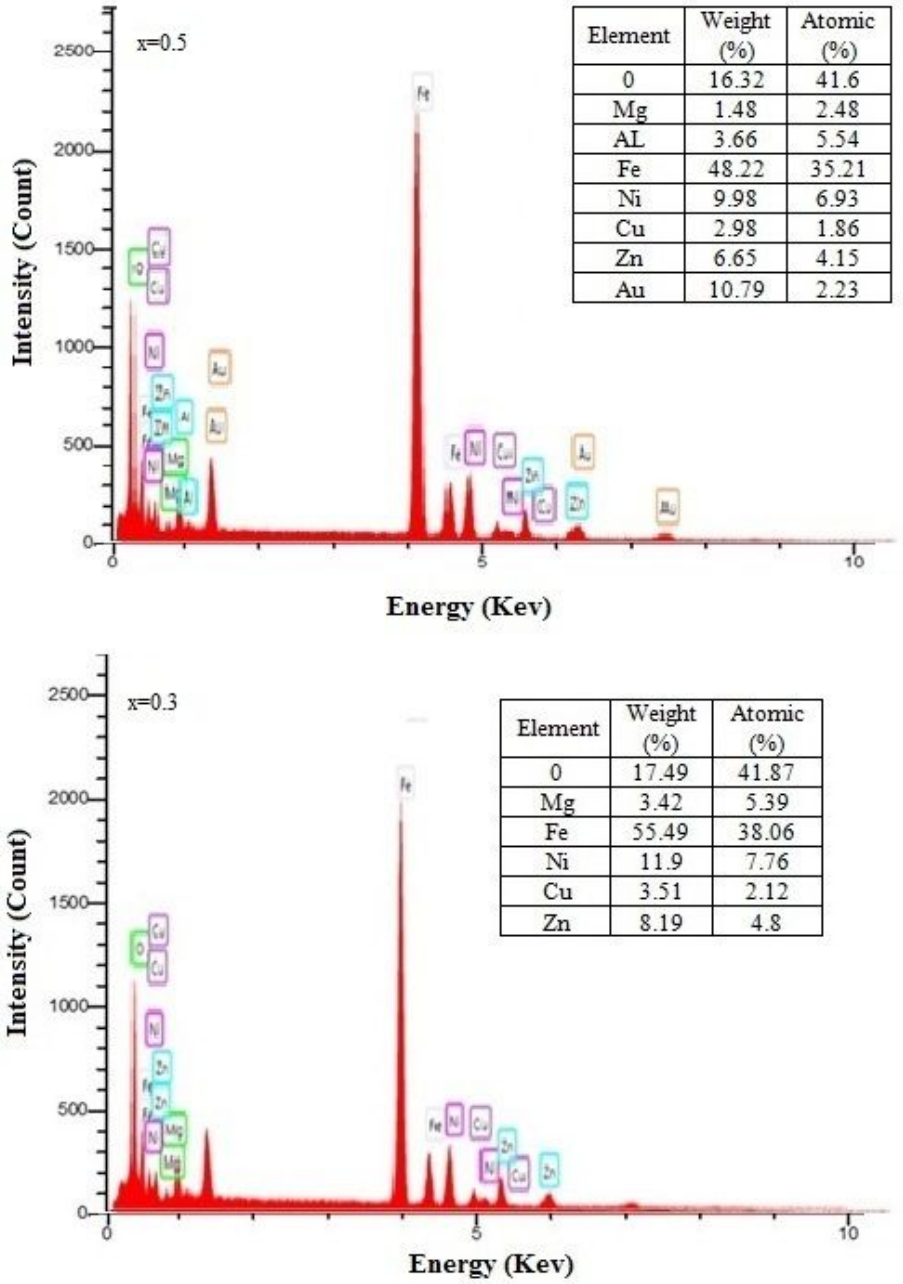

Element	Weight (%)	Atomic (%)
0	16.32	41.6
Mg	1.48	2.48
AL	3.66	5.54
Fe	48.22	35.21
Ni	9.98	6.93
Cu	2.98	1.86
Zn	6.65	4.15
Au	10.79	2.23

Element	Weight (%)	Atomic (%)
0	17.49	41.87
Mg	3.42	5.39
Fe	55.49	38.06
Ni	11.9	7.76
Cu	3.51	2.12
Zn	8.19	4.8

Figure 5

EDX spectrum of Ni1-x (Zn0.6 Mg0.2Cu0.2) x Fe2O4 with x equals to 0.3 and 0.5

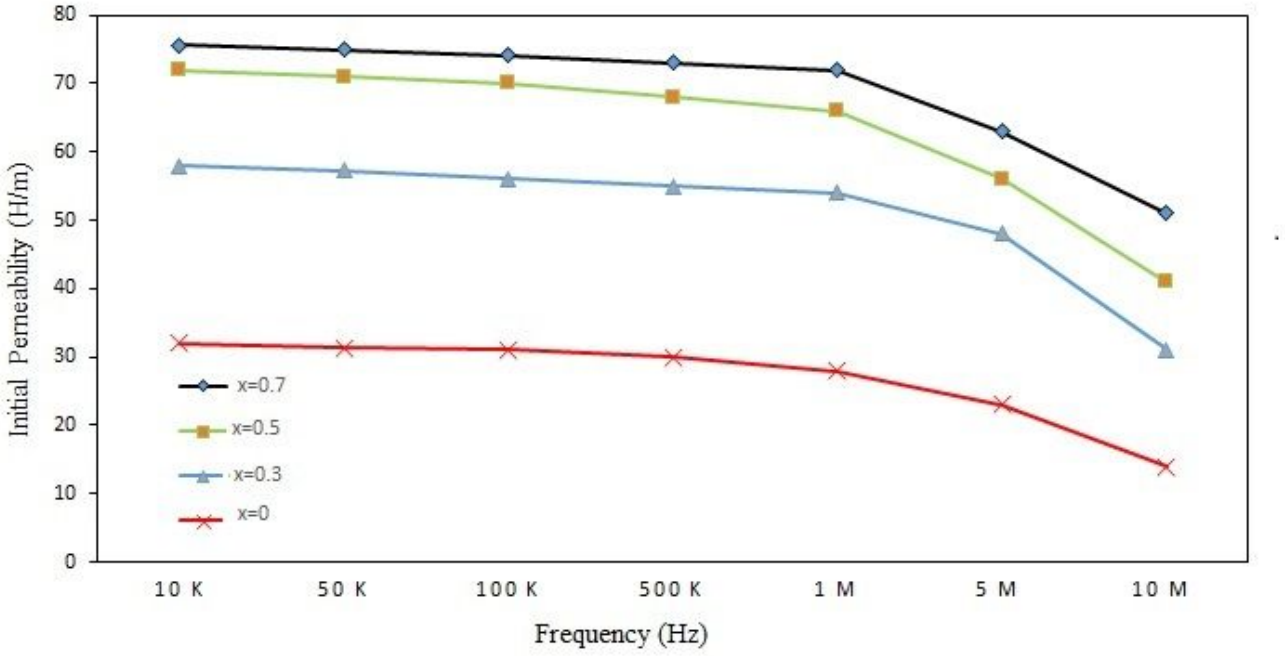

Figure 6

The variations of initial permeability concerning frequency for ferrite samples with x equal to 0.0, 0.3, 0.5, and 0.7.

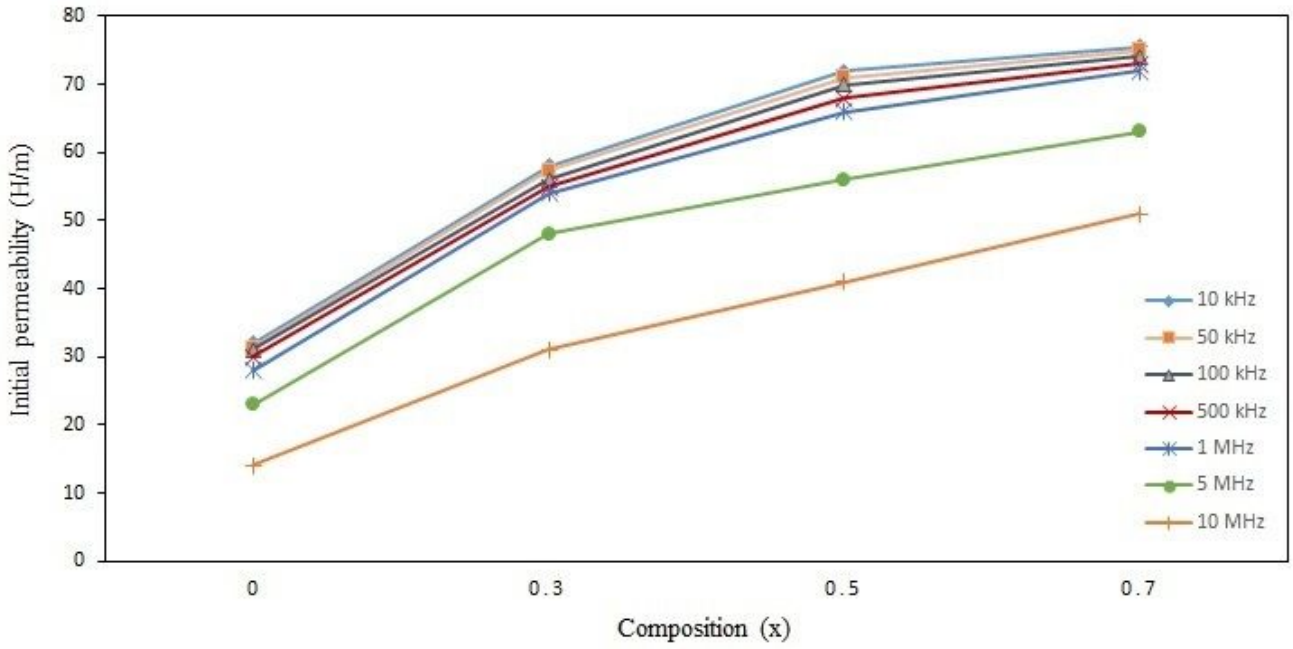

Figure 7

The variations of initial permeability concerning x values for Ni1-x (Zn0.6 Mg0.2Cu0.2) x Fe2O4.

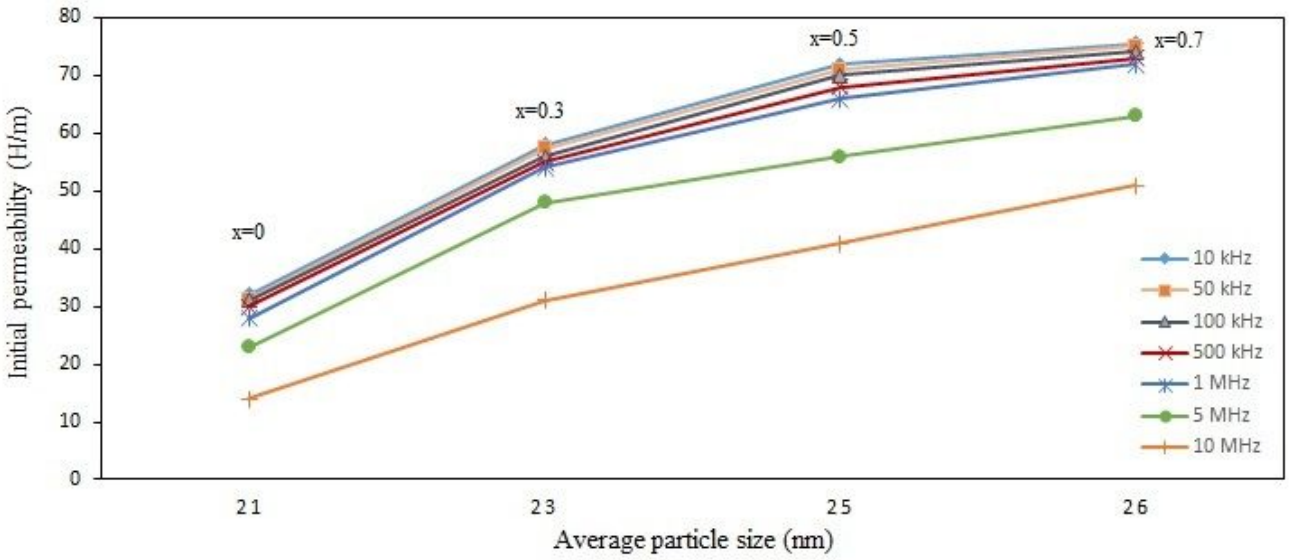

Figure 8

The variations of initial permeability as a function of mean particle size for Ni1-x (Zn0.6 Mg0.2Cu0.2) x Fe2O4.

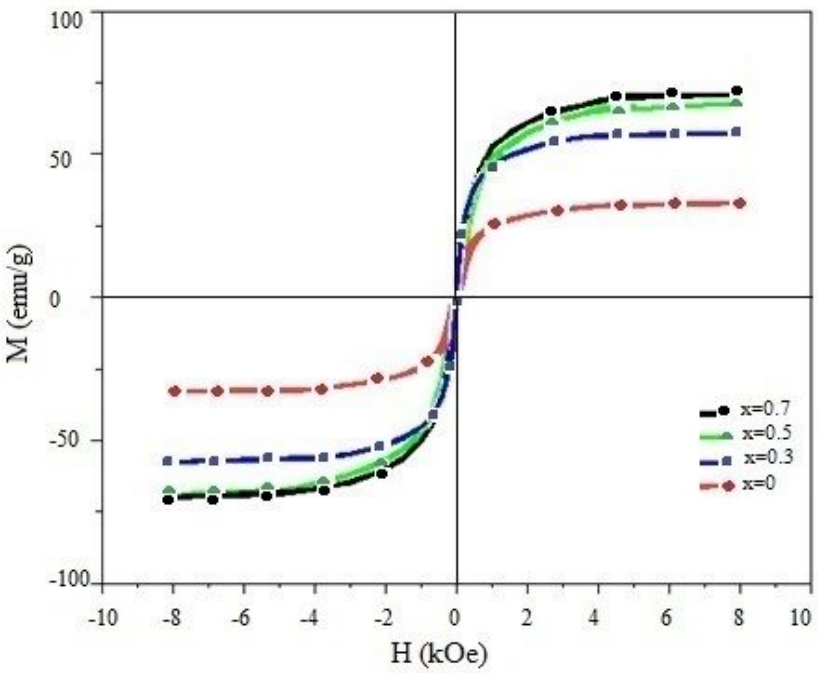

Figure 9

Room temperature hysteresis loops for Ni1-x (Zn0.6 Mg0.2Cu0.2) x Fe2O4 with x equal to: 0.0, 0.3, 0.5 and 0.7.

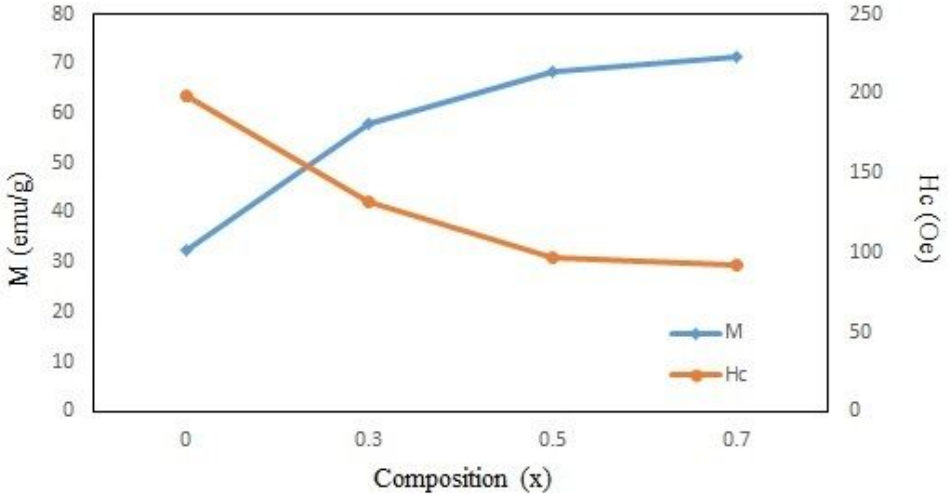

Figure 10

The variations of magnetization and coercivity of Ni1-x(Zn0.6 Mg0.2Cu0.2)xFe2O4 as a function of x.

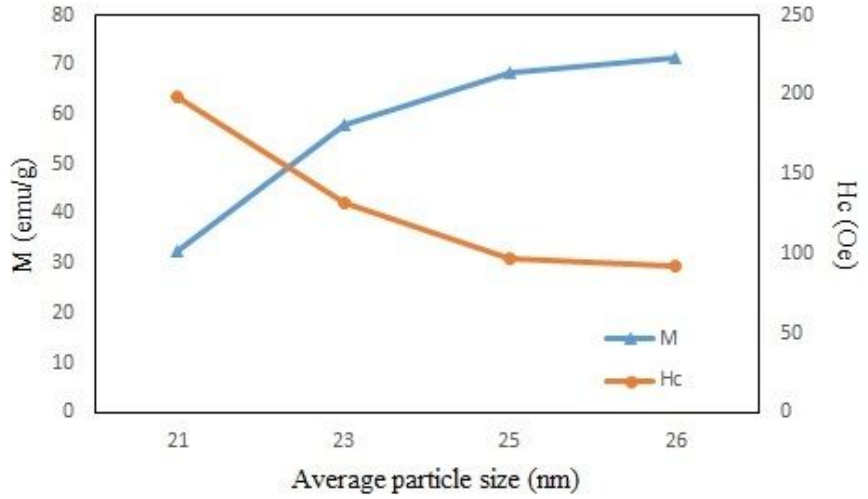

Figure 11

The variations of magnetization and coercivity of Ni1-x (Zn0.6 Mg0.2Cu0.2) x Fe2O4 as a function of average particle size.